Temperature- and Cost-Aware Design of 3D Multiprocessor Architectures

Ayse K. Coskun Andrew B. Kahng Tajana Simunic Rosing
University of California, San Diego
{acoskun, abk, tajana}@cs.ucsd.edu

Abstract— **3D stacked architectures provide significant benefits in performance, footprint and yield. However, vertical stacking increases the thermal resistances, and exacerbates temperature-induced problems that affect system reliability, performance, leakage power and cooling cost. In addition, the overhead due to through-silicon-vias (TSVs) and scribe lines contribute to the overall area, affecting wafer utilization and yield. As any of the aforementioned parameters can limit the 3D stacking process of a multiprocessor SoC (MPSoC), in this work we investigate the tradeoffs between cost and temperature profile across various technology nodes. We study how the manufacturing costs change when the number of layers, defect density, number of cores, and power consumption vary. For each design point, we also compute the steady state temperature profile, where we utilize temperature-aware floorplan optimization to eliminate the adverse effects of inefficient floorplan decisions on temperature. Our results provide guidelines for temperature-aware floorplanning in 3D MPSoCs. For each technology node, we point out the desirable design points from both cost and temperature standpoints. For example, for building a many-core SoC with 64 cores at 32nm, stacking 2 layers provides a desirable design point. On the other hand, at 45nm technology, stacking 3 layers keeps temperatures at an acceptable range while reducing the cost by an additional 17% in comparison to 2 layers.**

I. Introduction

With each new technology node, transistor size shrinks, the levels of integration increase, and consequently, a higher number of cores are integrated on a single die (e.g., Sun's 16-core Rock processor and Intel's 80-core Teraflop chip). Interconnects, on the other hand, have not followed the same trend as transistors. As a result, in the deep-submicron era a large portion of the total chip capacitance is due to interconnect capacitance. Interconnect length also has an adverse impact on performance. To compensate for this performance loss, repeaters are included in the circuit design, and interconnect power consumption rises further [16]. Vertical stacking of dies into a 3D architecture is a recently proposed approach to overcome these challenges associated with interconnects. With 3D stacking, interconnect lengths and power consumption are reduced. Another advantage of 3D stacking comes from silicon economics: individual chip yield, which is inversely dependent on area, increases when a larger number of chips with smaller areas are manufactured. On the other hand, as the number of chips integrated in the third dimension increases, the area overhead of the through-silicon-vias (TSVs) connecting the layers and of scribe lines becomes more noticeable, affecting overall system yield. Moreover, 3D integration can result in considerably higher thermal resistances and power densities, as a result of placing computational units on top of each other. Thermal hot spots due to high power densities are already a major concern in 2D chips, and in 3D systems the problem is more severe [21].

In this work, our goal is to investigate tradeoffs among various parameters that impose limitations on the 3D design. Specifically, we observe the effects of design choices for building 3D multicore architectures (i.e., number of cores, number of layers, process technology, etc.) on the thermal profile and on manufacturing cost. While investigating the thermal dynamics of 3D systems, we consider several performance-, temperature-, and area-aware floorplanning strategies, and evaluate their effectiveness in mitigating temperature-induced challenges. Following this study, we propose guidelines for temperature-aware floorplanning, and a temperature-aware floorplan optimizer. Using temperature-aware floorplanning, we eliminate the possible adverse effects of inefficient floorplanning strategies on temperature during our analysis on the cost-temperature tradeoff. The proposed analysis flow in our paper can be utilized for choosing beneficial design points that achieve the desired cost and temperature levels for the target process technology.

We make the following contributions in this project:

- For a given set of CPU cores and memory blocks in a multiprocessor architecture, we investigate yield and cost of 3D integration. Splitting the chip into several layers is advantageous for system yield and reduces the cost; however, the temperature becomes a limiting factor as the number of layers increases. We show the tradeoff between cost and temperature in 3D systems for various chip sizes across different technology nodes (i.e., $65nm$, $45nm$ and $32nm$). For example, for a many-core system with 64 cores, stacking 3 layers achieves \$77 and \$14 cost reduction for 65 and 45nm, respectively, in comparison to 2 layers. However, for 32nm, peak steady state temperature exceeds 85^oC for 3 layers, while only reducing manufacturing cost by \$3 per system. Therefore, as technology scaling continues and power density increases, conventional air-based cooling solutions may not be sufficient for stacking more than 2 layers.
- We investigate a wide set of floorplanning strategies in terms of their effects on temperature profiles. The floorplanning strategies we investigate include placing cores and memories in different layers (as in systems targeting multimedia applications with high memory bandwidth needs), homogeneously distributing cores and memory blocks, clustering cores in columns, and so on. We demonstrate that basic guidelines for floorplanning, such as avoiding placing cores on top of each other in adjacent layers, are sufficient to reach a close-to-optimal floorplan for multicore systems with 2 stacked layers. For higher numbers of layers, temperature-aware floorplanning gains in significance.
- We include the thermal effects and area overhead of through-silicon-vias (TSVs) in the experimental methodology. We show that for $65nm$, TSV densities limited to 1-2% of the area change the steady state temperature profile by only a few degrees. However, as technology scales down to $45nm$ or $32nm$, the thermal effects of TSVs become more prominent with a more noticeable impact on area as well.

The rest of the paper starts with an overview of prior work in analysis and optimization of 3D design. Section III discusses the experimental methodology, and in Section IV we provide the details of the modeling and optimization methods utilized in this work. Section V presents the experimental results, and Section VI concludes the paper.

II. Related Work

High temperatures have adverse effects on performance, as the effective operating speed of devices decreases with increasing temperature. In addition, leakage power has an exponential dependence on temperature. Thermal hot spots and large temperature gradients accelerate temperature-induced failure mechanisms, causing reliability degradation [15]. In this section, we first discuss previously proposed temperature-aware optimization methods for 3D design. We then provide an overview of cost and yield analysis.

Most of the prior work addressing temperature induced challenges in 3D systems has focused on design-time optimization, i.e., temperature-aware floorplanning. Floorplanning algorithms typically perform simulated annealing (SA) based optimization, using various kinds of floorplan representations (such as B*-Trees [5] or

Normalized Polish Expressions [23]). One of the SA-based tools developed for temperature-aware floorplanning in 2D systems is HotFloorplan [23].

Developing fast thermal models is crucial for thermally-aware floorplanning, because millions of configurations are generated during the SA process. Some of the typically used methods for thermal modeling are numerical methods (such as finite element method (FEM) [7]), compact resistive network [24], and simplified closed-form formula [6]. Among these FEM-based methods are the most accurate and the most computationally costly, whereas closed-form methods are the fastest but have lower accuracy.

In [8], Cong et al. propose a 3D temperature-aware floorplanning algorithm. They introduce a new 3D floorplan representation called combined-bucket-and-2D-array (CBA). The CBA based algorithm has several kinds of perturbations (e.g., rotation, swapping of blocks, interlayer swapping, etc.) which are used to generate new floorplans in the SA engine. A compact resistive thermal model is integrated with the 3D floorplanning algorithm to optimize for temperature. The authors also develop a hybrid method integrating their algorithm with a simple closed-form thermal model to get a desired tradeoff between accuracy and computation cost.

Hung et al. [14] take the interconnect power into account in their SA-based 3D temperature-aware floorplanning technique, in contrast to most of the previous work in this area. Their results show that excluding the interconnect power in floorplanning can result in under-estimation of peak temperature. In Healy et al.'s work on 3D floorplanning [11], a multi-objective floorplanner at the microarchitecture level is presented. The floorplanner simultaneously considers performance, temperature, area and interconnect length. They use a thermal model that considers the thermal and leakage inter-dependence for avoiding thermal runaway. Their solution consists of an initial linear programming stage, followed by an SA-based stochastic refinement stage.

Thermal vias, which establish thermal paths from the core of a chip to the outer layers, have the potential to mitigate the thermal problems in 3D systems. In [26], a fast thermal evaluator based on random walk techniques and an efficient thermal via insertion algorithm are proposed. The authors show that, inserting vias during floorplanning results in lower temperatures than inserting vias as a post-process.

Cost and yield analyses of 3D systems have been discussed previously, as in [18] and [10]. However, to the best of our knowledge, a joint perspective on manufacturing cost and thermal behavior of 3D architectures has not been studied before. In this work, we analyze the tradeoffs between temperature and cost with respect to various design choices across several different technology nodes. For thermally-aware floorplanning of MPSoCs, we compare several well-known strategies for laying out the cores and memory blocks against floorplanning with a temperature-aware optimizer. In our analysis, we use an optimization flow that minimizes the steady state peak temperature on the die while reducing the wirelength and footprint to achieve a fair evaluation of thermal behavior. Our experimental framework is based on the characteristics of real-life components, and it takes the TSV effects and leakage power into account.

III. Methodology

In this section we provide the details of our experimental methodology. In many-core SoCs, the majority of the blocks on the die are processor cores and on-chip memory (e.g., typically L2 caches). We do not take the other blocks (I/O, crossbar, memory controller, etc) into account in our experiments; however the guidelines we provide in this study and the optimization flow are applicable when other circuit blocks are included in the methodology as well.

A. Architecture and Power Consumption

We model a homogeneous multicore architecture, where all the cores are identical. We model the cores based on the SPARC core in Sun Microsystems's UltraSPARC T2 [19], manufactured at $65nm$ technology. The reason for this selection is that, as the number of cores increase in multicore SoCs, the designers integrate simpler cores as opposed to power-hungry aggressive architectures to achieve the desired tradeoff between performance and power consumption (e.g., Sun's 8-core Niagara and 16-core Rock processors).

The peak power consumption of SPARC is close to its average power value [17]. Thus, we use the average power value of $3.2W$ (without leakage) at $1.2GHz$ and $1.2V$ [17], [19]. We compute the leakage power of CPU cores based on structure areas and temperature. For the $65nm$ process technology, a base leakage power density of $0.5W/mm^2$ at $383K$ is used [3]. We compute temperature dependence using Eqn. (1), which is taken from the model introduced in [12]. β is set at 0.017 for the $65nm$ technology [12].

$$P_{leak} = P_{base} \cdot e^{\beta(T_{current} - T_{383})} \quad (1)$$

$$P_{base} = 0.5 \cdot Area \quad (2)$$

To model cores manufactured at $45nm$ and $32nm$ technology nodes, we use Dennard scaling supplemented by ITRS projections. If k is the feature size scaling per technology generation, according to Dennard scaling, for each generation we should observe that frequency increases by a factor of k, while capacitance and supply voltage decrease by a factor of k. ITRS projects that supply voltage almost flatlines as scaling continues, scaling less than 10% per generation. Using these guidelines, we set the dynamic average power values of cores as in Table I, based on the equation $P \propto CV^2f$.

TABLE I. Power Scaling

Node	Voltage	Frequency	Capacitance	Power
$65nm$	$1.2V$	$1.2GHz$	C	$3.2W$
$45nm$	$1.1V$	$1.7GHz$	$C/1.4$	$2.72W$
$32nm$	$1.0V$	$2.4GHz$	$C/1.96$	$2.27W$

Each L2 cache on the system is 1 MB (64 byte line-size, 4-way associative, single bank), and we compute the area and power consumption of caches using CACTI [25] for $65nm$, $45nm$ and $32nm$. At $65nm$ the cache power consumption is $1.7W$ per each L2 including leakage, and this value also matches with the percentage values in [17]. The power consumption of each cache block reduces to $1.5W$ and $1.2W$ for $45nm$ and $32nm$, respectively.

The area of the SPARC core in the $65nm$ Rock processor is $14mm^2$. For $45nm$ and $32nm$ process technologies, we scale the area of the core (i.e., area scaling is on the order of the square of the feature size scaling). The area of the cores and caches for each technology node are provided in Table II. As the area estimates for cores and caches are almost equal, we assume the core and cache areas for $65nm$, $45nm$, and $32nm$ are $14mm^2$, $7mm^2$, and $3.5mm^2$, respectively, for the sake of convenience in experiments. This work assumes pre-designed IP blocks for cores and memories are available for designing the MPSoC, so the area and dimensions of the blocks are not varied across different simulations. We assume a mesh network topology for the on-chip interconnects. Each core is connected to an L2 cache, where the L2 caches might be private or shared, depending on the area ratio of cores and memory blocks.

TABLE II. Core and Cache Area

Technology	Core Area	Cache Area
$65nm$	$14mm^2$	$14.5mm^2$
$45nm$	$6.7mm^2$	$6.9mm^2$
$32nm$	$3.4mm^2$	$3.59mm^2$

B. Thermal Simulation

HotSpot [24] provides temperature estimation of a microprocessor at component or grid level by employing the principle of electrical/thermal duality. The inputs to HotSpot are the floorplan, package and die characteristics and the power consumption of each component. Given these inputs, HotSpot provides the steady state and/or the transient temperature response of the chip. *HS3D* has

TABLE III. PARAMETERS FOR THE THERMAL SIMULATOR

Parameter	Value
Die Thickness (one stack)	$0.15mm$
Convection Capacitance	$140J/K$
Convection Resistance	$0.1K/W$
Interlayer Material Thickness (3D)	$0.02mm$
Interlayer Material Resistivity (without TSVs)	$0.25m\ K/W$

extended HotSpot to 3D architectures [13] by adding a suite of library functions. HS3D allows the simulation of multi-layer device stacks, allowing the use of arbitrary grid resolution, and offering speed increases of over 1000 X for large floorplans. HS3D has been validated through comparisons to a commercial tool, Flotherm, which showed an average temperature estimation error of 3^oC, and a maximum deviation of 5^oC [14].

We utilize HotSpot Version 4.2 [24] (grid model), which includes the HS3D features, and modify its settings to model the thermal characteristics of the 3D architectures we are experimenting with. Table III summarizes the HotSpot parameters. We assume that the thermal package has cooling capabilities similar to typical packages available in today's processors. We calculate the die characteristics based on the trends reported for $65nm$ process technology. Changing the simulator parameters to model different chips and packages affects the absolute temperature values in the simulation—e.g., thinner dies are easier to cool and hence result in lower temperatures, while higher convection resistance means that the thermal package's cooling capabilities are reduced and more hot spots can be observed. However, the relative relationship among the results presented in this work is expected to remain valid for similar multicore architectures.

HotSpot models the interface material between the silicon layers as a homogeneous layer (characterized by thermal resistivity and specific heat capacity values). To model the through-silicon-vias (TSV), we assume a homogeneous via density on the die. The insertion of TSVs is expected to change the thermal characteristics of the interface material, thus, we compute the "combined" resistivity of the interface material based on the TSV density. We compute the joint resistivity for TSV density values of $d_{TSV} = \{8, 16, 32, 64, 128, 256, 512\}$ per block; that is, a core or a memory block has d_{TSV} vias homogeneously distributed over its area. For example, in a 2-layered 3D system containing 16 SPARC cores and 16 L2 caches, there is a total of $16 \cdot d_{TSV}$ vias on the die. Note that even if we had wide-bandwidth buses connecting the layers, we would need a lot less than 256 or 512 TSVs per block. We assume that the effect of the TSV insertion to the heat capacity of the interface material is negligible, which is a reasonable assumption, considering the TSV area constitutes a very small percentage of the total material area.

Table IV shows the resistivity change as a function of the via density for a 2-layered 3D system with 16 cores and 16 caches. In our experiments, each via has a diameter of $10\mu m$ based on the current TSV technology, and the spacing required around the TSVs is also $10\mu m$. The area values in the table refer to the total area of vias, including the spacing.

TABLE IV. EFFECT OF VIAS ON THE INTERFACE RESISTIVITY

# Vias per Block	Via Area (mm^2)	Area Overhead (%)	Resistivity (mK/W)
0	0.00	0.00	0.25
8	0.12	0.05	0.248
16	0.23	0.10	0.247
32	0.46	0.20	0.245
64	0.92	0.40	0.24
128	1.84	0.79	0.23
256	3.69	1.57	0.21
512	7.37	3.09	0.19

IV. TEMPERATURE- AND COST-AWARE OPTIMIZATION

A. Yield and Cost Analysis of 3D Systems

Yield of a 3D system can be calculated by extending the negative binomial distribution model as proposed in [18]. Eqns. (3) and (4) show how to compute the yield for 3D systems with known-good-die (KGD) bonding and for wafer-to-wafer (WTW) bonding, respectively. In the equations, D is the defect density (typically ranging between $0.001/mm^2$ and $0.005/mm^2$ [18]), A is the total chip area to be split into n layers, α is the defect clustering ratio (set to 4 in all experiments, as in [22]), A_{tsv} is the area overhead of TSVs, and P_{stack} is the probability of having a successful stacking operation for stacking known-good-dies. We set P_{stack} to 0.99, representing a highly reliable stacking process. Note that for wafer-to-wafer bonding, per chip yield is raised to the nth power to compute the 3D yield. Wafer-to-wafer bonding typically incurs higher yield loss as dies cannot be tested prior to bonding. In this work, we only focus on die-level bonding.

$$Y_{system} = [1 + \frac{D}{\alpha}(\frac{A}{n} + A_{tsv})]^{-\alpha} {P_{stack}}^n \quad (KGD) \tag{3}$$

$$Y_{system} = \{[1 + \frac{D}{\alpha}(\frac{A}{n} + A_{tsv})]^{-\alpha}\}^n \quad (WTW) \tag{4}$$

The number of chips that can be obtained per wafer is computed using Eqn. (5) [9]. In the equation, R is the radius of the wafer and A_c is the chip area, including the area overhead of TSVs and scribe lines. The scribe line overhead of each chip is $L_s(2\sqrt{A/n} + L_s)$, where L_s is the scribe line width (set at $100\mu m$ in out experiments). Note that for a 3D system with n layers, the number of systems manufactured out of a wafer is $U_{3d} = U/n$. We assume a standard $300mm$ wafer size in all of the experiments.

$$U = \frac{\pi R}{A_c} - 2\pi\frac{R}{\sqrt{A_c}} + \pi \tag{5}$$

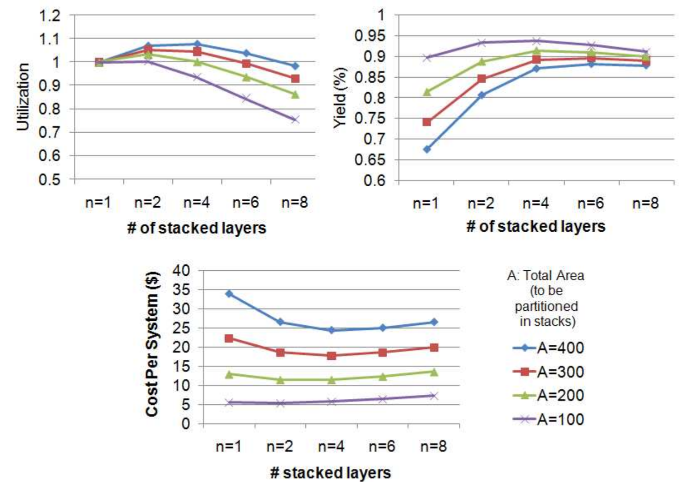

Fig. 1. Utilization, Yield and Cost ($). Utilization is normalized with respect to the 2D chip of equivalent total area.

Once we know the yield and wafer utilization, we compute the cost per 3D system using Eqn. (6), where C_{wafer} is the cost of the wafer in dollars. We set $C_{wafer} = \$3000$ in our experiments.

$$C = \frac{C_{wafer}}{U_{3d} \cdot Y_{system}} \tag{6}$$

The wafer utilization, yield and cost of systems with a total area ranging from $100mm^2$ to $400mm^2$ and with various numbers of stacked layers are provided in Figure 1. We observe that 3D stacking improves yield and reduces cost up to a certain number of stacked layers (n). As n is increased further, yield saturates and then drops mainly due to the drop in the probability of successfully stacking n layers (i.e., the P^n_{stack} parameter). These results for yield and cost motivate computing the desired cost-efficiency points for a given design before deciding on the number of layers and size of a 3D architecture. In addition, we see that partitioning chips with area $100mm^2$ and below does not bring benefits in manufacturing cost.

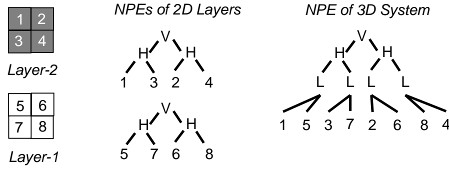

Fig. 2. Example NPE Representation.

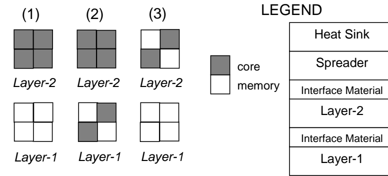

Fig. 3. Known-Good Floorplans for the Example Systems.

B. Temperature-Aware Floorplan Optimization

For a given set of blocks and a number of layers in the 3D system, we use HotFloorplan [23] for temperature-aware floorplan optimization. Using a simulated annealing engine, the HotFloorplan tool can move and rotate blocks, and vary their aspect ratios, while minimizing a pre-defined cost function.

A commonly used form of cost function in the literature (e.g., [11]) is shown in Eqn. (7), where a, b and c are constants, W is the wirelength, T is the peak temperature and A is the area. Minimizing f minimizes the communication cost and power consumption associated with interconnects, and also minimizes the chip area while reducing the peak temperature as much as possible.

$$f = a \cdot W + b \cdot T + c \cdot A \quad (7)$$

The wirelength component in Eqn. (7) only considers the wires connecting the cores and their L2 caches in this work. As we are integrating pre-designed core and cache blocks, the wirelengths within each block are the same across all simulations. To compute the wirelength, we calculate the Manhattan distance between the center of a core and the center of its L2 cache, and weigh this value based on the wire density between the two units. However, as we are experimenting with a homogeneous set of cores and caches, the wire density is the same across any two components, and is set to 1.

We use fixed aspect ratios of cores and memory blocks as in a real-life many-core SoC design scenario, where IP-cores and memories with pre-determined dimensions are integrated. This simplification reduces the simulation time for the floorplanner. Thus, instead of a two-phase optimization flow of partitioning and then floorplanning (e.g., [14], [1]), we are able to perform a one-shot optimization, where the blocks can be moved across layers in the annealing process.

HotFloorplan represents floorplans with Normalized Polish Expressions (NPEs), which contain a set of units (i.e., blocks in the floorplan) and operators (i.e., relative arrangement of blocks). The design space is explored by the simulated annealer using the following operators: (1) swap adjacent blocks, (2) change relative arrangement of blocks, and (3) swap adjacent operator and operand. For 3D optimization, we extend the algorithm in HotFloorplan with the following operators defined in [14]: (1) Move a block from one layer to another (interlayer move), and (2) Swap two blocks between 2 layers (interlayer swap). As we utilize fixed-size cores and caches in this paper, the interlayer move can be considered as an interlayer swap between a core or memory and a "blank" grid cell in the floorplan. These moves still maintain the NPEs, and satisfy the balloting property (which verifies the resulting NPE as valid) [1]. NPE representations for an example 3D system are provided in Figure 2. While the letters V and H demonstrate horizontal and vertical cuts, L represents different stacks in the system.

C. Sensitivity Analysis of the Optimizer

For verification of the optimizer, we compare the results obtained by the optimizer to known-best results for several experiments. We use smaller sample 3D systems to reduce the simulation time in the verification process. All samples are 2-layered 3D systems, and they have the following number of cores and caches: (1) 4 cores and 4 memory blocks, (2) 6 cores and 2 memory blocks, and (3) 2 cores and 6 memory blocks. The known-best results are computed by performing exhaustive search for a fixed footprint area. For each of the three cases, the optimizer result is the same as the result of the exhaustive search. The solutions for the example set are shown in Figure 3.

We also run a set of experiments for larger MPSoCs to verify the SA-based optimizer: an 8-core MPSoC and an 18-core MPSoC, both with 4 layers and with equal number of cores and L2 caches. In all of our experiments, we observe that optimal results avoid overlapping cores on adjacent layers on top of each other. Therefore, we only simulate floorplans that do not overlap cores in adjacent layers. When no cores can overlap, for a 4-layered system without any "blank" cells (i.e., the core and memory blocks fully utilize the available area) and with equal areas of caches and cores, there are 3^n different floorplans. The reason for the 3^n is that, considering a vertical column of blocks (i.e., blocks at the same grid location on each layer), there are 3 possible options of cache/core ordering, without violating the no-overlap restriction. These three possible orderings (from top layer to bottom layer) are: (1) C-M-C-M, (2) C-M-M-C, and (3) M-C-M-C, where M and C represent a memory block and a core, respectively.

For the 8-core MPSoC, we simulate all possible floorplans that abide by the restriction of not overlapping cores and that minimize the wirelength. This search constitutes a solution space of $3^4 = 81$ different designs, where all designs have 4 components on each layer (2x2 grid). For the 18-core MPSoC, similarly we have 9 components on each layer in a 3x3 grid, and we simulate 1000 randomly selected floorplans that maintain the same restriction for overlapping cores (among a solution space of 3^9 floorplans). In both experiments, we select the floorplan with the lowest steady state peak temperature at the end. The optimizer result is the same as the best floorplan obtained in the 8-core experiment. In the 18-core case, the optimizer results in 1.7^oC lower temperature than the best random solution.

As a second step in the verification process, we perform a study on how the coefficients in the cost function affect the results of the optimizer. This step is also helpful in the selection of coefficients. Note that the area (A) in Eqn. (7) is in hundreds of millimeters, temperature (T) in several hundred Kelvin degrees, and wirelength (W) is in tens of millimeters. The range of constants used in this experiment takes the typical values of A, T and W into account.

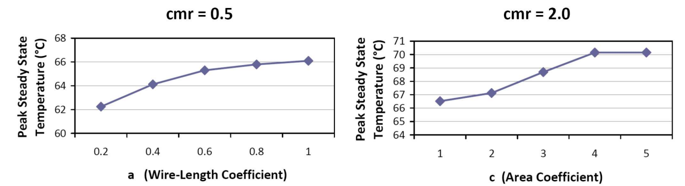

Fig. 4. Effect of Cost Function Parameters on Temperature.

Figure 4 demonstrates how the peak steady state temperature achieved by the floorplan changes when the wirelength coefficient (a) varies (other constants fixed), and when area coefficient (c) varies (again other constants fixed). Note that for a 2-layered system with an equal number of cores and memories, the optimizer minimizes the wirelength by placing a core and its associated L2 on top of each other. Therefore, changing the coefficient of the wirelength does not change the solution as placing a core and its L2 on top of each other provides the smallest total wire distance. To create a more interesting case for wirelength minimization, we use a 2-layered 3D system with core-to-memory ratio (CMR) of 0.5. For investigating the

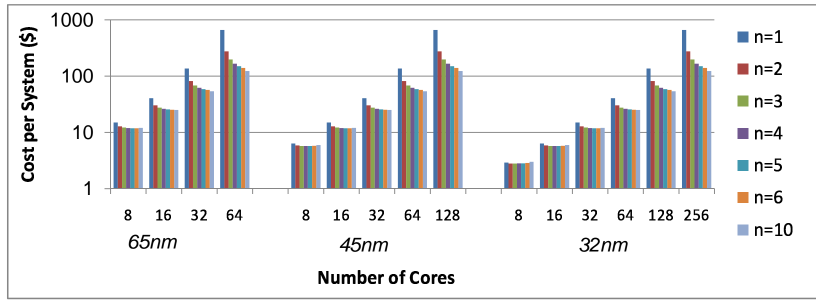

Fig. 5. Cost Change Across Technology Nodes.

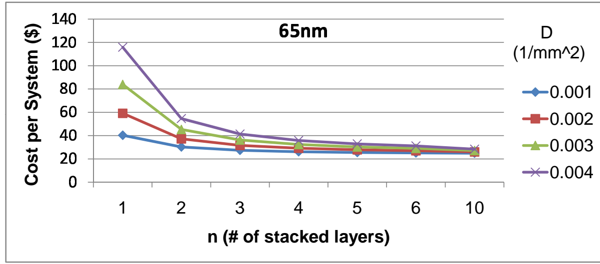

Fig. 6. Effect of Defect Density on System Cost.

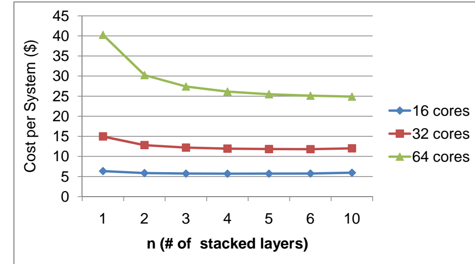

Fig. 7. Change in Cost with respect to Number of Cores and Layers.

effect of the area coefficient, we use fewer memory blocks than cores ($CMR = 2$), to see a more significant effect on peak temperature.

In HotFloorplan, the interconnect delay is computed using a first order model based on [2] and [20]. While more accurate delay models exist in literature, such as [4], in our experiments the first order model is sufficient. This is due to the fact that the floorplanner tends to place cores and their memories on adjacent layers and as close as possible to each other to reduce the wirelength (recall that the distance for vertical wires are much shorter than horizontal ones in general). Thus, increasing the accuracy of the wire delay model does not introduce noticeable differences in our experiments.

Based on the results presented, we selected the coefficients as $a = 0.4$, $b = 1$, and $c = 4$. Similar principles stated above can be utilized for selecting the coefficients for different 3D systems.

V. Experimental Results

In this section, we discuss the results of our analysis on the manufacturing cost and thermal behavior of 3D systems. First, we demonstrate how the cost changes depending on defect density, number of cores and number of layers for $65nm$, $45nm$ and $32nm$ technology nodes. We then evaluate various floorplanning strategies, and compare the results against our temperature-aware floorplanner. Finally, the section concludes by pointing out the tradeoffs between cost and temperature for a wide range of design choices, and providing guidelines for low-cost reliable 3D system design.

A. Design Space Exploration for 3D System Cost

We summarize the variation of cost across the process technologies $65nm$, $45nm$ and $32nm$ in Figure 5. In this experiment, the defect density is set at $0.001/mm^2$, and the core to memory ratio (CMR) is 1 (i.e., each core has a private cache). We compute the cost up to 256 cores for each node, but omit the results in the figure for the cases where per-system cost exceeds \$1000 (note that the y-axis is on a logarithmic scale). For building MPSoCs with a high number of cores, 3D integration becomes critical for achieving plausible system cost. Technology scaling provides a dramatic reduction in cost, assuming that the increase in defect density is limited.

Defect density is expected to increase as the circuit dimensions shrink. Thus, to evaluate how the cost is affected by the change in defect density (D), in Figure 6 we show the cost per system in dollars (y-axis), and the x-axis displays the number of stacked layers in the system (keeping the total area to be split the same). There are 16 cores and 16 memory blocks in the 3D architecture (i.e., $CMR = 1$), and the technology node is $65nm$. In all of the experiments in this section, the TSV count is set to a fixed number of 128 per chip. Especially if the defect density is high, 3D integration brings significant benefits. For example, for a defect density of $0.003/mm^2$, splitting the 2D system into 2 layers reduces the cost by 46%, and splitting into 4 layers achieves a cost reduction of 61%. In the rest of the experiments we use a defect density of $0.001/mm^2$, representing mature process technologies.

In Figure 7, we demonstrate the change of cost with respect to the number of layers and number of cores for 32nm technology. The CMR is again 1 in this experiment. For the 16-core system, the minimum cost is achieved for 4 layers, and for the 32-core case integrating 6 layers provides the minimum system cost. As the number of cores, or in other words, total area increases, we may not reach the minimum point for the cost curve by integrating a reasonable number of layers—e.g., for 64 cores, integrating 10 layers seems to give the lowest cost in the figure, which may result in unacceptable thermal profiles. Therefore, especially for many-core systems, an optimization flow that considers both the cost and temperature behavior is needed, as increasing the number of stacked layers introduces conflicting trends in thermal behavior and yield.

We observe that TSVs do not introduce noticeable impact on yield and cost, as long as the ratio of TSV area to chip area is kept lower than only a few percents. For $45nm$ technology, the cost difference between a fixed TSV count of 128 and a fixed TSV percentage of 1% is shown in Figure 8. n demonstrates the number of layers as before. For example, when we compare keeping the TSV density at 1% of the chip area against using a fixed number (i.e., 128) of TSVs per chip, up to 64 cores, the cost difference between the two cases is below \$1. As the number of cores and overall area increase, accommodating TSVs occupying 1% of the chip area translates to integrating thousands of TSVs. Thus, for many-core systems, TSV overhead becomes a limiting factor for 3D design.

B. Thermal Evaluation of 3D Systems

In this section, we evaluate the thermal behavior for various design choices in 3D systems. To understand the effects of temperature-

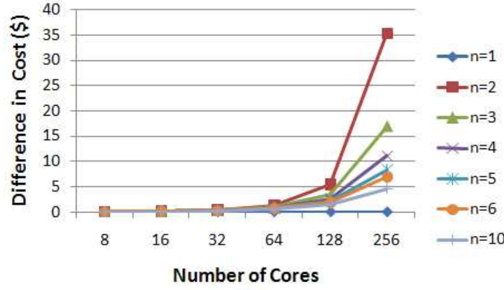

Fig. 8. TSV cost difference between using a fixed count and a fixed percentage (45nm).

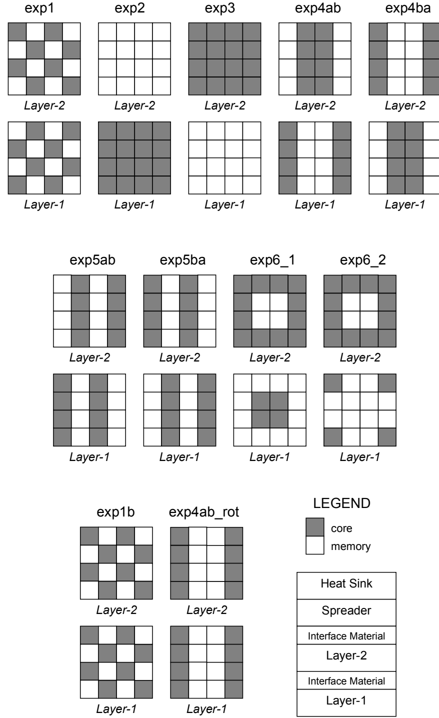

Fig. 9. Floorplans.

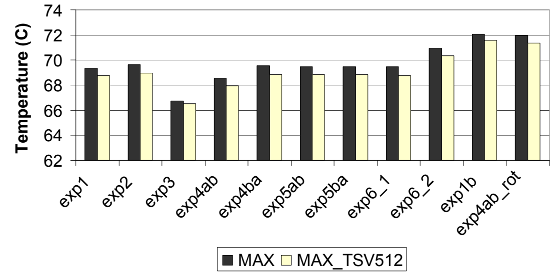

Fig. 10. Peak Steady State Temperature Comparison.

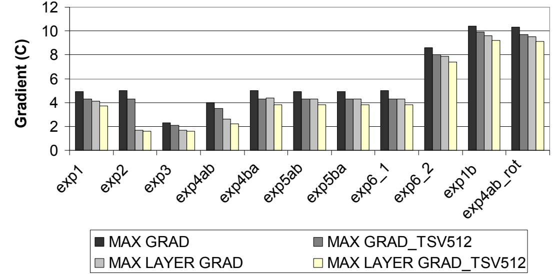

Fig. 11. Comparison of Gradients.

aware optimization and also to ensure that our results are not biased by floorplanning decisions, we first analyze the effects of 3D floorplanning on temperature. All the simulation results shown in this section are for the $65nm$ technology.

1) Comparing Floorplanning Strategies: To investigate how floorplanning affects the thermal profile, we experiment with a 16-core system with the architectural characteristics described in Section III. Each core has an L2 cache, so we have a total of 16 cores and 16 memory blocks. The various floorplans we use in our simulations are summarized in Figure 9.

Figure 10 demonstrates the peak steady state temperature achieved by each floorplan. *MAX* shows the results without considering the TSV modeling, and *MAX_TSV512* represents the results that take into account the TSV effect on temperature, with TSV density of 512 per block. Even though 512 vias per block is a significantly large number, there is only a slight reduction in the steady state peak temperature (i.e., less than 1^oC). For this reason, we do not plot the thermal results with all the TSV densities that we experiment with. For the rest of the results, we use a TSV density of 512 per block, representing a best-case scenario for temperature.

For the 2-layer 3D system, *exp3*, which places all the cores on the layer adjacent to the heat spreader and all memories in the lower layer, has the lowest temperature. *exp4ab* also achieves significant reduction of peak temperature in comparison to other strategies, and the wirelength is the same. Note that in both floorplans the core can be overlapped in adjacent layers with its L2 cache. All the floorplans that increase the peak temperature (e.g., *exp1b*) have overlapping cores in adjacent layers.

In addition to thermal hot spots, large spatial gradients (i.e., temperature differences among different locations on the chip) cause challenges in performance, reliability and cooling efficiency, so gradients with lower magnitudes are preferable. In Figure 11, we compare the maximum spatial gradient among the blocks at steady state. *MAX GRAD* and *MAX LAYER GRAD* represent the gradient across all blocks (considering all layers) and the maximum intra-layer gradient (the gradients across layers are not taken into account), respectively. The traces with the *_TSV* suffix are from the simulations including the TSV modeling. We see that *exp3* also outperforms the other strategies for reducing the gradients on the die.

2) The Effect of the Ratio of Core and Memory Area: In Section V-B.1, all the 3D systems have an equal number and area of cores and memories. Next, we look into how the change in CMR affects the thermal behavior. For this experiment, we simulate various CMR values, but we only show the results for $CMR = 2$ and $CMR = 0.5$ as the trends for other ratios are similar.

In Figures 12 and 13, we compare the peak temperature and largest gradient for the floorplans generated by the optimizer for core-to-memory area ratios of 2, 0.5, and 1 (baseline). While the peak temperature is positively correlated with the number of cores, the temperature gradients increase when the CMR is different than 1. Thus, separating the core and memory layers as much as possible is a good solution for reducing the gradients as well.

For 2-layered 3D architectures, following basic guidelines such as avoiding a vertical overlap of cores (or in general, power-hungry units), and placing the units with higher power consumption closer to the heat sink achieve very similar results to the known-best solutions. These two principles prove to be more significant than avoiding the placement of cores in adjacent locations horizontally in a multicore 3D system. This general rule-of-thumb holds for any CMR value. When $CMR < 1$, separating the cores on the same layer as much as possible is also necessary for achieving better thermal profiles.

3) The Effect of the Number of Stacks on Temperature: The purpose of the next experiment is to observe the effect of increasing

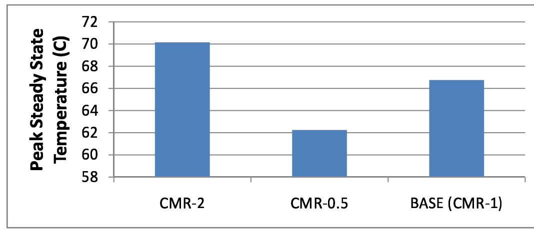

Fig. 12. Comparison of Peak Temperature - Core to Memory Area Ratio.

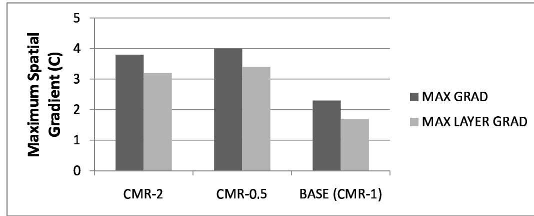

Fig. 13. Comparison of Gradients - Core to Memory Area Ratio.

the number of stacks on peak steady state temperature and the temperature gradients. We compare a 2-layered 3D stack architecture against a 4-layered architecture using the same number of cores and memories to achieve a fair comparison. In other words, the total power consumption of the cores and memories are the same in the 2- and 4-layered systems in Figure 14.

Figure 14 compares the peak steady state temperature of the 2- and 4-layered systems for several floorplanning strategies shown in Figure 9. In the 4-layered systems, the floorplanning patterns for upper and lower layers are repeated; e.g., for *exp3*, we have a core layer, a memory layer, again a core layer and a memory layer (ordered from top layer to bottom). In Figure 15, we demonstrate the spatial gradients on the systems. For the 4-layered systems, we observe a significant increase in the gradients across the chip (i.e., MAX_GRAD). This is because the temperature difference between the layers close to and far away from the heat sink increases with higher number of layers in the 3D stack.

In the example shown in Figures 14 and 15, for the 4-layered stack the footprint reduces by 44% and the system cost decreases by close to 40% in comparison to using a 2-layered stack (i.e., for a system that contains the same number of cores and caches). On the other hand, we see a noticeable increase in temperature. Hence, for multicore systems, temperature-aware floorplanning becomes crucial for systems with a higher number of stacked layers.

4) Optimizer Results: We have seen in the last section that for 3D systems with a high number of vertical layers, temperature-aware optimization is a requirement for reliable design. Figure 16 compares the optimizer results for a 4-layered 3D system (containing 16 cores and 16 L2 caches) to the best performing custom strategies investigated earlier. All the floorplans investigated in Figure 16 have the same footprint. This is an expected result as we keep the dimensions of the memory blocks and cores fixed during optimization, and the optimization flow (which minimizes the total area as well) results in the same footprint area as the hand-drawn methods. We show the resulting floorplan of the optimizer in Figure 17, where the darker blocks are cores, and Layer-4 is the layer closest to heat sink. Note that there are other floorplans that have the same lowest steady state peak temperature.

For 4-layered systems, the optimizer achieves an additional 5% of peak temperature reduction in comparison to the best performing hand-drawn floorplan. The benefits of optimization are more substantial for a higher number of stacked layers. As the number of layers increases, reducing the peak steady state temperature through floorplan optimization becomes more critical for reducing the adverse effects of high temperatures at runtime—this is because the dynamic

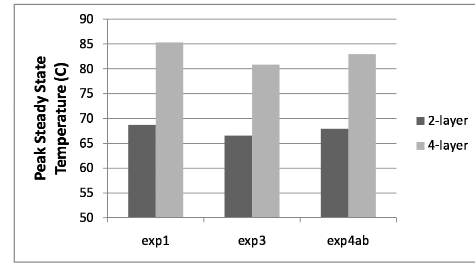

Fig. 14. Comparison of 2- and 4-Layered Systems.

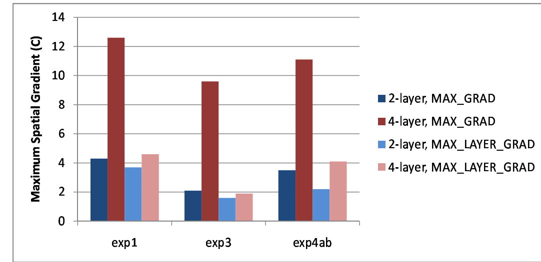

Fig. 15. Comparison of Spatial Gradients in 2- and 4-Layered Systems.

temperature range at runtime is highly dependent on the steady state behavior of the system.

Even though we do not explicitly model the interconnect power consumption, the accuracy impact of this is expected to be minimal. This is because all of the floorplanning strategies in this example (i.e., both custom designed strategies and the optimizer results) place cores and their associated L2 caches on adjacent layers, and overlap them to minimize the total amount of interconnects. As noted earlier, the TSV length is dramatically less than the horizontal interconnects, as the thickness of the interlayer material is $0.02mm$.

C. Investigating the Temperature-Cost Trade-Off

Next we discuss the design tradeoff between cost and temperature profiles for $65nm$, $45nm$ and $32nm$ technology nodes. Figure 18 demonstrates the cost per system in dollars and the peak steady state temperature for the system with 64 cores and 64 L2 caches. All the thermal results in this section utilize the temperature-aware floorplan optimizer discussed previously.

The common trend in the figure is that, going from a single layer chip to 2 layers, both the cost and temperature decrease considerably. The decrease in temperature is a result of the vertical heat transfer from the cores to their memories, which have considerably lower temperatures. Thus, in addition to dissipating heat through the heat spreader and sink, the cores transfer part of their heat to their caches and end up with several degrees of cooler temperature. However, if 3D stacking overlaps cores in the adjacent layers (e.g., in the case where the number of cores is more than that of caches), steady state temperature is expected to increase.

Also, note that the cost per system drops significantly with each process technology. This sharp drop results from the simultaneous increase in yield and wafer utilization when the same chip is manufactured at a smaller technology node.

Another important observation regarding Figure 18 is that, for $65nm$ and $45nm$, it is possible to reduce the per-system cost significantly by partitioning the system into 3 layers; i.e, \$77 and \$14 reduction for $65nm$ and $45nm$, respectively, in comparison to building the same system with 2 layers. However, for $32nm$, peak steady state temperature exceeds 85^oC for $n = 3$, while only reducing the cost by approximately \$3. Therefore, as technology scaling continues and power density increases, it may not be feasible to stack more than 2 layers for systems with conventional cooling.

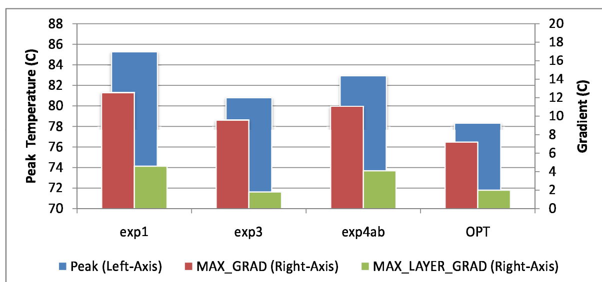

Fig. 16. Peak Temperature and Gradients - Comparison to Optimizer Results.

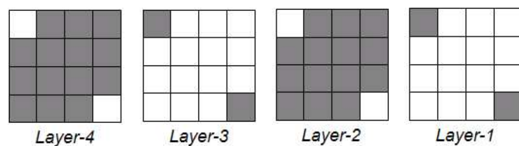

Fig. 17. Optimizer Result for the 4-Layered 16 Core MPSoC.

Also, the heat density increases rapidly for a higher number of cores. 3D integration for many-core systems in $45nm$ and below will require more efficient cooling infrastructures, such as liquid cooling.

VI. Conclusion

3D integration is a promising solution for shortening wirelength, and for reducing the power consumption and delay of interconnects on SoCs. In addition, partitioning large chips into several layers increases yield and reduces the cost. One critical issue in 3D design is that vertical stacking exacerbates the challenges associated with high temperatures.

In this work, we presented an analysis infrastructure, evaluating both manufacturing cost and temperature profile of 3D stack architectures across current and future technology nodes. We utilized a temperature-aware floorplanner to eliminate any adverse effects of inefficient placement while evaluating the thermal profile. As a result of our floorplanning study, we have provided guidelines for thermal-aware floorplanning in 3D architectures. For 3D systems with more than 2 layers, we showed that using an optimizer provides significant advantages for reducing peak temperature.

Using our framework, we presented experimental results for a wide range of assumptions on process technology characteristics and design choices. For example, for a 45nm many-core SoC with 64 cores, stacking 3 layers cuts the manufacturing cost in half compared to a single-layer chip, while still maintaining a peak temperature below 85^oC. When the same system is manufactured at 32nm, stacking 2 layers and 3 layers reduces the cost by 25% and 32%, respectively, compared to the 2D chip. However, at 32nm, the steady state peak temperature for 3 layers reaches 87^oC, due to the increase in the power density. Such results emphasize that using a joint evaluation of cost and temperature is critical to achieve cost-efficient and reliable 3D design.

Acknowledgements

The authors would like to thank Prof. Yusuf Leblebici at EFPL for his valuable feedback. This work has been funded in part by Sun Microsystems, UC MICRO, Center for Networked Systems (CNS) at UCSD, MARCO/DARPA Gigascale Systems Research Center and NSF Greenlight.

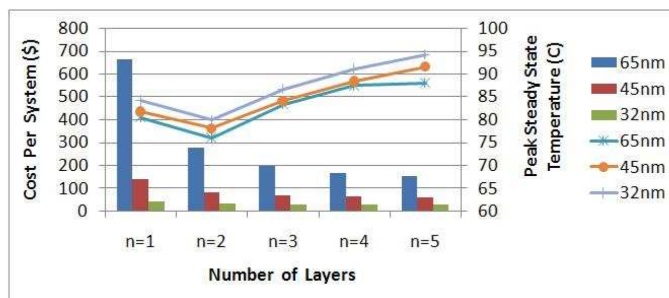

Fig. 18. Cost and Temperature for a 64-Core MPSoC: bar graphs show cost on the left y-axis, and line graphs show peak temperature on the right axis.

References

[1] M. Awasthi, V. Venkatesan and R. Balasubramonian. Understanding the Impact of 3D Stacked Layouts on ILP. *Journal of Instruction Level Parallelism*, 9:1–27, 2007.
[2] K. Banerjee and A. Mehrotra. Global (interconnect) Warming. *IEEE Circuits and Devices Magazine*, 17:16–32, September 2001.
[3] P. Bose. Power-Efficient Microarchitectural Choices at the Early Design Stage. In *Keynote Address, Workshop on Power-Aware Computer Systems*, 2003.
[4] L. Carloni, A. B. Kahng, S. Muddu, A. Pinto, K. Samadi and P. Sharma. Interconnect Modeling for Improved System-Level Design Optimization. In *ASP-DAC*, pages 258–264, 2008.
[5] Y.-C. Chang, Y.-W. Chang, G.-M. Wu and S.-W. Wu. B*-Trees: A New Representation for Non-Slicing Floorplans. In *DAC*, pages 458–463, 2000.
[6] T. Chiang, S. Souri, C. Chui and K. Saraswat. Thermal Analysis of Heterogenous 3D ICs with Various Integration Scenarios. *International Electron Devices Meeting (IEDM) Technical Digest*, pages 31.2.1–31.2.4, 2001.
[7] W. Chu and W. Kao. A Three-Dimensional Transient Electrothermal Simulation System for ICs. In *THERMINIC Workshop*, pages 201–207, 1995.
[8] J. Cong, J. Wei and Y. Zhang. A Thermal-Driven Floorplanning Algorithm for 3D ICs. In *ICCAD*, pages 306–313, 2004.
[9] D. K. de Vries. Investigation of Gross Die per Wafer Formula. *IEEE Trans. on Semiconductor Manufacturing*, 18(1):136–139, 2005.
[10] C. Ferri, S. Reda and R. I. Bahar. Parametric Yield Management for 3D ICs: Models and Strategies for Improvement. *J. Emerg. Technol. Comput. Syst.(JETC)*, 4(4):1–22, 2008.
[11] M. Healy, M. Vittes, M. Ekpanyapong, C. S. Ballapuram, S. K. Lim, H.-H. S. Lee and G. H. Loh. Multiobjective Microarchitectural Floorplanning for 2-D and 3-D ICs. *IEEE Transactions on CAD*, 26(1):38–52, Jan 2007.
[12] S. Heo, K. Barr and K. Asanovic. Reducing Power Density Through Activity Migration. In *ISLPED*, pages 217–222, 2003.
[13] HS3D Thermal Modeling Tool. http://www.cse.psu.edu/ link/hs3d.html.
[14] W.-L. Hung, G.M. Link, Y. Xie, V. Narayanan and M.J. Irwin. Interconnect and Thermal-Aware Floorplanning for 3D Microprocessors. In *ISQED*, pages 98–104, 2006.
[15] *Failure Mechanisms and Models for Semiconductor Devices*. JEDEC publication JEP122C. http://www.jedec.org.
[16] P. Kapur, G. Chandra and K. Saraswat. Power Estimation in Global Interconnects and Its Reduction Using a Novel Repeater Optimization Methodology. In *DAC*, pages 461–466, 2002.
[17] A. Leon, J.L. Shin, K.W. Tam, W. Bryg, F. Schumacher, P. Kongetira, D. Weisner and A. Strong. A Power-Efficient High-Throughput 32-Thread SPARC Processor. *ISSCC*, 42(1):7–16, Jan. 2006.
[18] P. Mercier, S.R. Singh, K. Iniewski, B. Moore and P. O'Shea. Yield and Cost Modeling for 3D Chip Stack Technologies. In *IEEE Custom Integrated Circuits Conference (CICC)*, pages 357–360, 2006.
[19] U. Nawathe, M. Hassan, L. Warriner, K. Yen, B. Upputuri, D. Greenhill, A. Kumar and H. Park. An 8-Core 64-Thread 64-bit Power-Efficient SPARC SoC. *ISSCC*, pages 108–590, Feb. 2007.
[20] R. H. J. M. Otten and R. K. Brayton. Planning for Performance. In *DAC*, pages 122–127, 1998.
[21] K. Puttaswamy and G. H. Loh. Thermal Herding: Microarchitecture Techniques for Controlling Hotspots in High-Performance 3D-Integrated Processors. In *HPCA*, pages 193–204, 2007.
[22] S. Reda, G. Smith and L. Smith. Maximizing the Functional Yield of Wafer-to-Wafer 3D Integration. *To appear in IEEE Transactions on VLSI Systems*, 2009.
[23] K. Sankaranarayanan, S. Velusamy, M. Stan and K. Skadron. A Case for Thermal-Aware Floorplanning at the Microarchitectural Level. *The Journal of Instruction-Level Parallelism*, 8:1–16, 2005.
[24] K. Skadron, M.R. Stan, W. Huang, S. Velusamy, K. Sankaranarayanan and D. Tarjan. Temperature-Aware Microarchitecture. In *ISCA*, pages 2–13, 2003.
[25] D. Tarjan, S. Thoziyoor and N. P. Jouppi. CACTI 4.0. Technical Report HPL-2006-86, HP Laboratories Palo Alto, 2006.
[26] E. Wong and S. Lim. 3D Floorplanning with Thermal Vias. In *DATE*, pages 878–883, 2006.